

Dual Pose-invariant Embeddings: Learning Category and Object-specific Discriminative Representations for Recognition and Retrieval

Rohan Sarkar, Avinash Kak

Electrical and Computer Engineering, Purdue University, USA

{sarkarr, kak}@purdue.edu

Abstract

In the context of pose-invariant object recognition and retrieval, we demonstrate that it is possible to achieve significant improvements in performance if both the category-based and the object-identity-based embeddings are learned simultaneously during training. In hindsight, that sounds intuitive because learning about the categories is more fundamental than learning about the individual objects that correspond to those categories. However, to the best of what we know, no prior work in pose-invariant learning has demonstrated this effect. This paper presents an attention-based dual-encoder architecture with specially designed loss functions that optimize the inter- and intra-class distances simultaneously in two different embedding spaces, one for the category embeddings and the other for the object level embeddings. The loss functions we have proposed are pose-invariant ranking losses that are designed to minimize the intra-class distances and maximize the inter-class distances in the dual representation spaces. We demonstrate the power of our approach with three challenging multi-view datasets, ModelNet-40, ObjectPI, and FG3D. With our dual approach, for single-view object recognition, we outperform the previous best by 20.0% on ModelNet40, 2.0% on ObjectPI, and 46.5% on FG3D. On the other hand, for single-view object retrieval, we outperform the previous best by 33.7% on ModelNet40, 18.8% on ObjectPI, and 56.9% on FG3D.

1. Introduction

Pose-invariant recognition and retrieval [7] is an important problem in computer vision with practical applications in robotic automation, automatic checkout systems, and inventory management. The appearance of many objects belonging to the same general category can vary significantly from different viewpoints, and, yet, humans have no difficulty in recognizing them from arbitrary viewpoints. In pose-invariant recognition and retrieval, the focus is on mapping

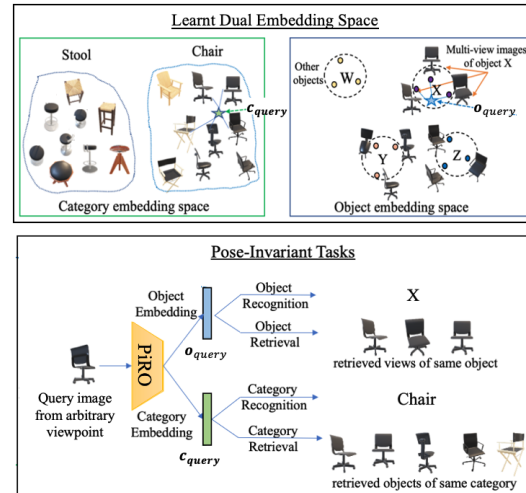


Figure 1. The upper panel shows objects belonging to two different categories, chair and stool. In the proposed disentangled dual-space learning, the goal for the learning of category-based embeddings is to capture what maximally discriminates the objects belonging to the two categories — the presence or the absence of the back-rest. On the other hand, the object-identity based embeddings are meant to capture what is distinctive about each object. The lower panel illustrates our dual-space approach for simultaneously learning the embeddings in two different spaces for category and object-identity-based recognition and retrieval tasks.

the object images to embedding vectors such that the embeddings for the objects that belong to the same category are pulled together for all the available viewpoints in relation to the embeddings for the objects for the different categories.

Our work demonstrates that the performance of pose-invariant learning as described above can be significantly improved if we disentangle the category-based learning from the object-identity-based learning.

Fig. 1 illustrates what we mean by disentangling the category-based representation from the object-identity-based representation. Assume that an object database contains images of different types of chairs and different types of stools. We would want our network to learn the category-based embedding vectors for the chair class and for the stool

class. These embeddings need to capture what is maximally discriminating between the chairs and the stools — the presence or the absence of a back-rest. At the same time, we would want the network to learn object-identity based embeddings. These embeddings should represent what is distinctive about each object type in relation to all other objects types in the same category. For example, in the chair category, we would want the network to be able to discriminate between, say, lounge chairs and desk chairs.

Prior work [6, 10, 22, 26] has employed multi-view deep networks to learn aggregated multi-view representations capturing the variability in object appearance under different pose transformations. While these methods demonstrate good performance in category-level tasks when multiple views of objects are available during inference, *their performance degrades when only a single view is available*. Since real-world applications often necessitate inference from single views, Ho et al. [7] proposed a family of pose-invariant embeddings for both recognition and retrieval by imposing constraints such that the single-view embeddings of an object are clustered around its multi-view embeddings, which in turn are clustered around a proxy embedding representing the associated high-level category that the object belongs to. However, this approach does not do a good enough job of separating the embeddings for two different objects that belong to the same category (e.g., two different types of chairs, two different types of kettles, etc.). As a result, prior approaches perform well on category-level tasks but not on object-level tasks, as we will demonstrate later in our experimental results (see Tables 2, 3).

Here is arguably the most significant difference between the previous methods and the one being proposed in this paper: *Rather than learning representations that capture both category-specific and object-specific discriminative features within the same embedding space, we simultaneously learn them in two distinct embedding spaces*, as depicted in the lower panel in Fig. 1. In one space that is devoted to category-based representations, objects from the same category can be closely embedded together, capturing shared characteristics among them, while in the other space, the one for object identity-based representations, embeddings for the different object types (within the same category or otherwise) are allowed to be as separated as dictated by the attributes that differentiate them. This strategy enables our network to learn object representations that are more discriminative overall. This should explain the superior performance of our framework in both recognition and retrieval, especially for the more difficult case when only a single-viewpoint query image is available. For single-view object recognition, we get an improvement in accuracy of 20.0% on ModelNet40, 46.5% on FG3D, and 2.0% on ObjectPI. Along the same lines, for the case of single-view object retrieval, we achieve a significant mAP improvement

of 33.7% on ModelNet-40, 56.9% on FG3D, and 18.8% on ObjectPI datasets.

In order to learn the dual embeddings simultaneously, we propose an encoder that we refer to as the Pose-invariant Attention Network (PAN). PAN uses a shared CNN backbone for capturing visual features common to both the category and the object-identity based representations from a set of images of an object recorded from different view-points. The visual features are then mapped to separate low-dimensional category and object-identity based embeddings using two fully connected layers. PAN also aggregates visual features of objects from different views using self-attention to generate what we call multi-view embeddings. The dual embeddings, defined in Section 3, can be used for *both category and object-level recognition and retrieval from single and multiple views*.

For training the network, we propose two pose-invariant category and object-identity based losses that are jointly optimized to learn the dual embeddings. The pose-invariant category loss clusters together the instances of different objects belonging to the same category while separating apart the instances from different categories in the category embedding space. On the other hand, the pose-invariant object-identity based loss clusters together the instances that carry the same object-identity label and separates what would otherwise be mutually confusing object instances with two different object-identity labels from the same category in the object embedding space.

2. Background and Related work

(A) Ranking and proxy-based losses: Ranking losses, used in deep metric learning, focus on optimizing the relative pair-wise distances between exemplars (pairs [2], triplets [8] or quadruplets [1]), such that similar samples are pulled closer and dissimilar samples are pushed apart. For ranking losses, the selection of informative exemplars [4, 5, 9, 16, 19, 21, 23, 24, 27] is crucial, which however incurs additional computational costs and memory. To reduce the training complexity, proxy-based approaches [14] define a proxy embedding for each class and optimize sample-to-proxy distances. However, they only capture relationships between samples and the proxies, which are less informative compared to the extensive sample-to-sample relations inherent in pair-based losses, which is particularly important for fine-grained tasks.

(B) Multi-view and Pose-Invariant Classification and Retrieval: In multi-view object recognition and retrieval [6, 10, 22, 26], each object from category c is captured from a set of V views and is denoted by $\mathbf{X} = \{\mathbf{x}_k\}_{k=1}^V$. For each object, a set of single-view embeddings are extracted by inputting each image \mathbf{x}_k to a network g_s , which are then aggregated to generate multi-view embeddings as $g_m(\mathbf{X}) = \Phi(\{g_s(\mathbf{x}_k)\}_{k=1}^V)$, where Φ denotes the aggreg-

gation operation. Multi-view losses cluster the multi-view embeddings of objects from the same category together and yield good performance on category-based tasks when multiple views of objects are available during inference. However, they perform poorly when only a single view is available during inference as the single-view embeddings are not constrained to be close to the multi-view embeddings in the embedding space. To mitigate this, the approach by [7] learns pose-invariant embeddings by combining two separate view-to-object and object-to-category models trained using different types of pose-invariant losses. These losses optimize the pose-invariance distance defined as

$$d^{pi}(\mathbf{x}, \mathbf{X}, \mathbf{p}_c) = \alpha d(g_s(\mathbf{x}), g_m(\mathbf{X})) + \beta d(g_m(\mathbf{X}), \mathbf{p}_c) \quad (1)$$

where, α promotes the clustering of single-view embeddings around the object’s multi-view embedding, while β encourages the clustering of the multi-view embedding of the object around the learned proxy embedding \mathbf{p}_c for its category c . However, these losses do not effectively separate embeddings of distinct objects from the same category, as we will demonstrate later in Fig. 5. This results in poor performance on object-based tasks.

In summary, prior work focused primarily on learning category-specific embeddings, with the object-to-object variations within each category represented by the variations in the embedding vectors within the same embedding space. In contrast, we learn a unified model that explicitly decouples the object and category embeddings. The model is trained jointly using two proposed pose-invariant ranking losses. In the category embedding space, the proposed loss clusters instances of different objects belonging to the same category together. In the object embedding space, the proposed loss clusters different views of the same object while separating confusing instances of different objects from the same category, thereby capturing discriminatory features to distinguish between similar objects from the same category. This significantly improves object recognition and retrieval performance over prior methods (ref. Tables 2, 3).

(C) Attention-based architectures: Since the advent of ViT [3], transformers have become increasingly popular for a variety of computer vision tasks. Most relevant to our work are hybrid architectures comprising a CNN backbone in conjunction with a transformer encoder that use multi-head attention layers to learn aggregated representations from image collections comprising different items [17, 18] and multi-view 3D shape representations [15, 25] for classification and retrieval tasks. In contrast, we only use a single-head self-attention layer for each subspace to aggregate visual features extracted from a DNN across different views to learn multi-view embeddings. The architectures in [15, 25] learn multi-view shape representations for category-based tasks and require multi-view images at inference time. In contrast, our dual-encoder is designed

to simultaneously learn pose-invariant category and object representations that can be utilized for both category and object-based tasks from single and multiple views during inference. Separate models for classification and retrieval tasks were proposed in [18], whereas our unified model can address both tasks jointly. Also, positional encodings are utilized by [3, 15] to preserve input order, but not by [18]. We omit positional encodings to ensure that the learned representations are independent of the input view order.

3. Proposed Approach

A high-level overview of our framework PiRO for learning dual pose-invariant representations of objects is shown in Fig. 2. Our approach learns by comparing pairs of objects belonging to the same category, while taking into account their multi-view appearances. This is illustrated in Fig. 2 where we show two different kettles, obviously belonging to the same category, and, in the depiction in the figure, we use three randomly chosen viewpoint images for each kettle. For the purpose of explanation, we have labeled the two objects as a and b . In general, we choose V number of randomly selected images from the different viewpoints for each object. The objective of this within-category learning is to become aware of the common attributes shared by these objects, like the spout, lid, handle, and overall body structure, enabling their categorization as a kettle.

The multi-view images are input to our proposed dual-encoder PAN, which we introduce in Section 3.1. The dual encoder consists of a shared CNN backbone responsible for capturing common visual features, along with two distinct heads dedicated to the learning of the dual category and object-identity based embeddings.

The encoder is trained jointly using pose-invariant losses designed for each respective embedding space, as described in Section 3.2. In the category embedding space, the loss is designed to cluster together the embeddings of the ob-

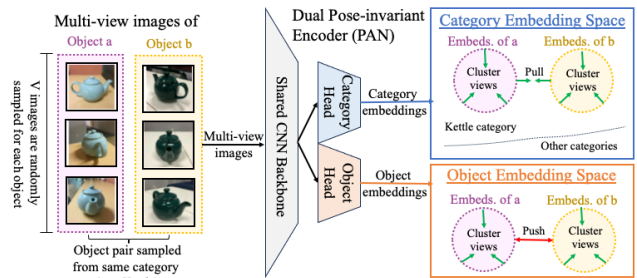


Figure 2. An overview of our PiRO framework to learn the dual pose-invariant object and category embeddings using losses specifically designed for each embedding space. Multi-view images of two randomly chosen objects from the same category are used to learn common characteristics of the objects in the category embedding space and discriminatory attributes to distinguish between them in the object embedding space.

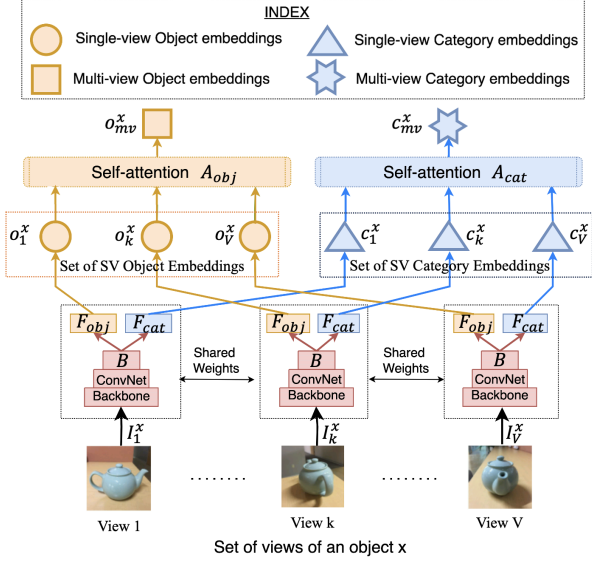


Figure 3. The Pose-invariant Attention Network (PAN) takes a set of multi-view images of an object as input, producing both single-view and multi-view embeddings for each representational subspace. The object embeddings are depicted in orange, while the category embeddings are in blue.

jects from the same category regardless of the viewpoints, as shown in top-right of Fig. 2. On the other hand, in the object-identity embedding space, the loss is designed to cluster together the embeddings for the instances that carry the same object-identity label, again regardless of the viewpoints, while separating instances with different object-identity labels from the same category, as shown in bottom-right of Fig. 2. The idea is for the encoder to capture shared characteristics among objects within the same category in the category space and discriminatory attributes to distinguish between them in the object space. These dual embeddings can then be utilized for pose-invariant category and object-based recognition and retrieval.

3.1. Pose-invariant Attention Network (PAN):

Fig. 3 illustrates in greater detail the design of PAN, the Pose-invariant Encoder shown previously in Fig. 2. It consists of a CNN backbone (B), two FC layers (F_{obj} and F_{cat}) and two single-head self-attention layers (A_{obj} and A_{cat}). It takes as input an unordered set of images from V different views of an object x from category l_x represented as $\mathbf{I}_{set}^x = \{\mathbf{I}_1^x, \dots, \mathbf{I}_k^x, \dots, \mathbf{I}_V^x\}$. The backbone and FC layers for each view share the same weights.

The backbone learns visual features common to both the category and object-identity representations. The visual features extracted from each object view are subsequently input to the FC layer (F_{obj}) to generate the object-identity embeddings. The set of *single-view object embeddings* for object x is denoted by:

$$\mathcal{E}_{obj}^x = \{\mathbf{o}_k^x \mid \mathbf{o}_k^x = F_{obj}(B(\mathbf{I}_k^x)) \quad \forall \mathbf{I}_k^x \in \mathbf{I}_{set}^x\} \quad (2)$$

Similarly, the shared visual features are input to another FC layer (F_{cat}) to generate category embeddings. The set of *single-view category embeddings* for object x is denoted by:

$$\mathcal{E}_{cat}^x = \{\mathbf{c}_k^x \mid \mathbf{c}_k^x = F_{cat}(B(\mathbf{I}_k^x)) \quad \forall \mathbf{I}_k^x \in \mathbf{I}_{set}^x\} \quad (3)$$

The single-view object and category embeddings are then passed into the self-attention layers A_{obj} and A_{cat} to learn the corresponding multi-view embeddings. The self-attention mechanism allows weighted interactions between the features extracted from one view with features extracted from all the remaining views in the set to capture the correlation between visual features across multiple views effectively. The resulting feature vectors from the images of an object are then aggregated using mean-pooling to get the multi-view embeddings. The resulting *multi-view object and category embedding* for object x is denoted by:

$$\mathbf{o}_{mv}^x = \frac{1}{V} \sum_{k=1}^V A_{obj}(\mathcal{E}_{obj}^x), \quad \mathbf{c}_{mv}^x = \frac{1}{V} \sum_{k=1}^V A_{cat}(\mathcal{E}_{cat}^x) \quad (4)$$

3.2. Pose-invariant Losses

The single-view and multi-view embeddings extracted using PAN are used for constructing pose-invariant losses that train the encoder to map object images across different viewpoints to compact low-dimensional subspaces, where the Euclidean distance between embeddings corresponds to a measure of object similarity across viewpoints. We propose two such pose-invariant losses for the object and category embedding spaces next.

(A) Pose-invariant Object Loss: This loss is designed specifically for fine-grained object recognition and retrieval from arbitrary viewpoints. The loss pulls together the embeddings of the different views of the same object, as shown by the green arrows in Fig. 4(A). This allows the encoder to learn common view-invariant features from multiple views. At the same time, it is designed to increase the inter-class distances between the embeddings (as shown by the red arrows in the same figure). That allows the encoder to learn the discriminative features to distinguish between visually similar objects from the same category.

Let us consider a pair of objects (a, b) from the same high-level category as shown in Fig. 4(A). The object-identity embeddings generated by the encoder (ref. Eqn. 2) from V views for each of the objects are symbolically represented as the two sets \mathcal{E}_{obj}^a and \mathcal{E}_{obj}^b respectively. For each such pair, embeddings of different objects with the minimum separation between them are the most informative and are chosen as the *confusers*. These embeddings are called confusers because they maximally violate the inter-class margin between the object pair and are the most likely to confuse a classifier. The confusers denoted by \mathbf{o}_{con}^a and

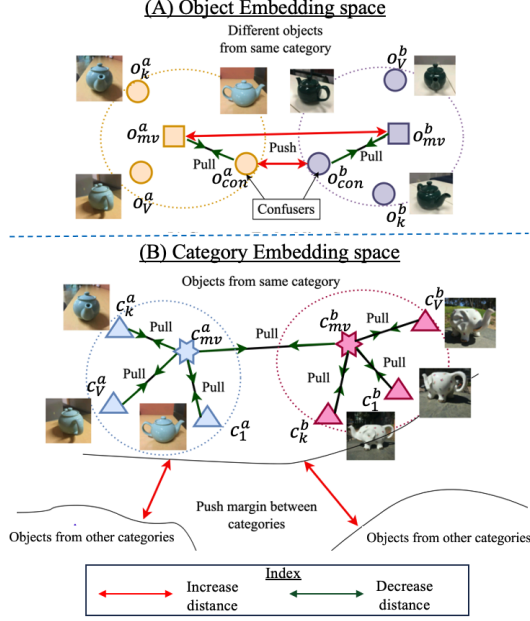


Figure 4. The pose-invariant losses enhance intra-class compactness and inter-class separation in the dual embedding spaces. In the object embedding space (top), confusing instances of two different objects from the same category are separated. In the category embedding space (bottom), objects belonging to the same category are pulled closer while being separated from those belonging to other categories.

\mathbf{o}_{con}^b are computed as

$$\mathbf{o}_{con}^a, \mathbf{o}_{con}^b = \underset{\forall \mathbf{x} \in \mathcal{E}_{obj}^a, \forall \mathbf{y} \in \mathcal{E}_{obj}^b}{\operatorname{argmin}} d(\mathbf{x}, \mathbf{y}) \quad (5)$$

where, $d(\mathbf{x}, \mathbf{y}) = \|\mathbf{x} - \mathbf{y}\|_2$ is the euclidean distance between the embeddings \mathbf{x} and \mathbf{y} . The multi-view object embeddings $\mathbf{o}_{mv}^a, \mathbf{o}_{mv}^b$ from the respective object-identity classes are considered as *positives*.

The intra-class compactness and inter-class separability are controlled using two margins α and β respectively. Our pose-invariant object-identity loss has two components:

(i) **Clustering loss** ensures that the distance between the multi-view embedding and the single-view confuser embedding in Eqn. 5 of the same object-identity class a does not exceed the margin α . For the object-identity class a , it is defined as:

$$\mathcal{L}_{intra}^a = \left[d(\mathbf{o}_{mv}^a, \mathbf{o}_{con}^a) - \alpha \right]_+ \quad (6)$$

where, $[z]_+ = \max(z, 0)$ is the hinge loss.

(ii) **Separation loss** ensures that the minimum distance between the single-view confuser embeddings of two objects a and b and also the separation between the multi-view object embeddings of the corresponding objects is greater than a margin β . By separating the confusers and multi-view embeddings of two objects from the same category, the encoder

will learn discriminatory features. It is defined as:

$$\mathcal{L}_{inter}^{a,b} = \left[\beta - d(\mathbf{o}_{con}^a, \mathbf{o}_{con}^b) \right]_+ + \left[\beta - d(\mathbf{o}_{mv}^a, \mathbf{o}_{mv}^b) \right]_+ \quad (7)$$

The overall loss is defined as:

$$\mathcal{L}_{piobj}^{a,b} = \mathcal{L}_{intra}^a + \mathcal{L}_{intra}^b + \mathcal{L}_{inter}^{a,b} \quad (8)$$

(B) **Pose-invariant Category Loss:** As shown by the green arrows in Fig. 4(B), this loss ensures that in the category embedding space, the single-view and multi-view embeddings of an object are well clustered and the multi-view embeddings for two different object-identity classes from the same category are embedded close to each other and do not exceed a margin θ . The clustering loss for the category embeddings (ref. Eqn. 3) of the objects a, b from the same category is defined as:

$$\mathcal{L}_{picat}^{a,b} = \left[d_{sm}^a - \theta \right]_+ + \left[d_{sm}^b - \theta \right]_+ + \left[d(\mathbf{c}_{mv}^a, \mathbf{c}_{mv}^b) - \theta \right]_+ \quad (9)$$

where, $d_{sm}^x = \frac{1}{V} \sum_{k=1}^V d(\mathbf{c}_k^x, \mathbf{c}_{mv}^x)$ is the mean of the distances between the multi-view and single-view embeddings for an object x in the category embedding space.

(C) **Total loss:** In the category embedding space, we use the large-margin softmax (L-Softmax) loss for separating the embeddings of objects from different categories (shown by the red arrows in Fig. 4(B)) using a margin γ . The dual-encoder PAN is jointly trained using all the losses and the overall loss is defined as

$$\mathcal{L} = \frac{1}{|\mathcal{P}|} \sum_{(a,b) \in \mathcal{P}} \mathcal{L}_{cat}^a + \mathcal{L}_{cat}^b + \mathcal{L}_{picat}^{a,b} + \mathcal{L}_{piobj}^{a,b} \quad (10)$$

where, $\mathcal{L}_{cat}^x = \frac{1}{V} \sum_{k=1}^V \mathcal{L}_\gamma(\mathbf{c}_k^x, l_x)$ such that $\mathcal{L}_\gamma(\mathbf{c}_k^x, l_x)$ is the L-Softmax loss [11] with margin γ for a category embedding \mathbf{c}_k^x of an object x belonging to category l_x from any viewpoint k , and \mathcal{P} is the set of all object pairs where each pair is randomly sampled from the same category.

4. Experiments

In this section, we evaluate our approach on pose-invariant classification and retrieval (PICR) tasks on three multi-view object datasets, report ablation studies at the end of this section, and additional results in the supplementary material.

(A) Setup, implementation details and results:

Datasets: ModelNet-40 [26] is a multi-view dataset comprising 3983 objects (3183 train and 800 test) with roughly 100 unique CAD models per category from 40 common object categories. The dataset is generated by starting from an arbitrary pose and rotating each CAD model every 30 degrees resulting in 12 poses per model. The ObjectPI dataset

Dataset	Embed. Space	Classification (Accuracy %)					Retrieval (mAP %)				
		Category		Object		Average	Category		Object		Average
		Single-view	Multi-view	Single-view	Multi-view		Single-view	Multi-view	Single-view	Multi-view	
ObjectPI	Single	69.56 ± 0.9	80.27 ± 1.9	88.35 ± 0.3	98.98 ± 0.9	84.29 ± 0.7	65.81 ± 0.5	75.60 ± 0.7	68.55 ± 0.5	99.46 ± 0.5	77.35 ± 0.4
	Dual	70.22 ± 0.7	82.48 ± 1.0	93.07 ± 0.8	98.64 ± 0.5	86.10 ± 0.3	65.20 ± 0.4	82.80 ± 0.5	80.61 ± 0.5	99.46 ± 0.3	82.02 ± 0.3
ModelNet	Single	85.09 ± 0.3	88.08 ± 0.6	82.90 ± 1.5	86.75 ± 1.2	85.71 ± 0.5	78.88 ± 0.2	82.88 ± 0.2	61.89 ± 2.3	91.22 ± 0.8	78.71 ± 0.7
	Dual	84.96 ± 0.2	88.32 ± 0.4	94.14 ± 0.3	96.88 ± 0.2	91.07 ± 0.2	79.30 ± 0.2	85.28 ± 0.4	84.46 ± 0.2	98.17 ± 0.1	86.80 ± 0.1
FG3D	Single	78.18 ± 0.2	80.42 ± 0.1	26.51 ± 0.3	29.76 ± 0.7	53.72 ± 0.3	65.05 ± 0.3	69.28 ± 0.2	15.79 ± 0.1	41.98 ± 0.6	48.02 ± 0.3
	Dual	78.89 ± 0.2	81.81 ± 0.1	83.00 ± 0.2	91.56 ± 0.1	83.81 ± 0.1	67.95 ± 0.3	74.24 ± 0.3	72.78 ± 0.3	95.47 ± 0.1	77.61 ± 0.2

Table 1. Pose-invariant Classification and Retrieval results on category and object-level tasks using our method for single and dual embedding spaces on the ModelNet-40, FG3D and ObjectPI datasets. The average performance along with standard deviation are reported.

[7] consists of images collected in the wild, by placing each object in a natural scene and capturing pictures from 8 views around the object, for 480 objects (382 train and 98 test) from 25 categories. We use the same training and test splits provided by [7] for both datasets. Additionally, we also evaluate our method on FG3D [12] which is a large-scale dataset for fine-grained object recognition with 12 views per object for 25552 objects (21575 training and 3977 test) from 66 categories.

Tasks: Ho et al. [7] proposed five tasks: *Single-view and multi-view category recognition*. These tasks predict the category from a single view and a set of object views respectively. *Single-view and multi-view category retrieval*. The goal of these tasks is to retrieve images from the same category as the query object from a single view and multiple views respectively. *Single-view object retrieval*. This task aims to retrieve other views of the same object in the query view. We additionally report results using our method in Table 1 on three more tasks which are extensions of the above-mentioned tasks. These tasks are *single and multi-view object recognition* and *multi-view object retrieval*. The splits for evaluation on all these tasks will be publicly released. Classification and retrieval performance are reported as accuracy and mean average precision (mAP) respectively.

Training details: Images are resized to 224×224 and normalized before being input to the network. The VGG-16 network [20] is used as the CNN backbone for a fair comparison with other state-of-the-art approaches. The last FC layers are modified to generate 2048-D embeddings and are initialized with random weights. A single layer and single head self-attention layer is used with a dropout of 0.25. The network is jointly trained using the proposed pose-invariant category and object losses. For all datasets, we set the margins $\alpha = 0.25, \beta = 1.00$ for the object embedding space and margins $\theta = 0.25, \gamma = 4.00$ for the category embedding space. We use the Adam optimizer with a learning rate of $1e^{-5}$ for ObjectPI, ModelNet-40, and $5e^{-5}$ for FG3D. We train for 25 epochs and use the step scheduler that reduces the learning rate by half after every 5 epochs.

(B) Comparison with state-of-the-art: In Table 2, we compare performance of our method against several state-of-the-art multi-view and pose-invariant methods [6, 7, 22] reported by [7] on the ModelNet-40 and ObjectPI datasets. For the single-view object recognition task, we report the results using the trained models provided by [7]. As explained in Section 2(B), the multi-view methods are designed for category-based tasks when multiple images are available during inference. However, they perform poorly when only a single view is available and Pose-invariant (PI) methods outperform the multi-view (MV) methods on single-view tasks as they constrain the single-view embeddings to be clustered close to the multi-view embeddings. Although these pose-invariant methods encourage the clustering of different views of the same object, they don’t effectively separate the confusing instances of neighboring objects from the same category in the embedding space. Hence, they don’t capture discriminative features to distinguish between visually similar objects from the same category because of which they exhibit poor performance on the single-view object recognition and retrieval tasks.

We observe that our method PiRO-DE, outperforms the state-of-the-art methods on both the average classification (improvement of 7.7% on ModelNet-40 and 2.6% on ObjectPI) and retrieval tasks (improvement of 13.0% on ModelNet-40 and 8.8% on ObjectPI) when learning dual category and object embeddings. We notice a significant improvement in the single-view object recognition (accuracy improves by 20.0% on ModelNet40 and 2.0% on ObjectPI) and retrieval tasks (mAP improves by 33.7% on ModelNet-40 and 18.8% on ObjectPI). Even in the single embedding space, PiRO-SE shows improvements on object-based tasks compared to the state-of-the-art approaches.

We train the state-of-the-art pose-invariant methods [7] on the FG3D dataset and compare performance with our method in Table 3. FG3D is more challenging for object-level tasks as it comprises a large number of similar objects in each category with fine-grained differences. As mentioned earlier, prior methods mainly focus on learn-

Method	ModelNet-40 (12 views)								ObjectPI (8 views)							
	Classification (Accuracy %)				Retrieval (mAP %)				Classification (Accuracy %)				Retrieval (mAP %)			
	SV Cat	MV Cat	SV Obj	Avg	SV Cat	MV Cat	SV Obj	Avg	SV Cat	MV Cat	SV Obj	Avg	SV Cat	MV Cat	SV Obj	Avg
MV-CNN	71.0	87.9	65.6	74.8	41.7	71.5	29.6	47.6	62.1	74.1	75.8	70.7	53.8	72.3	42.6	56.2
PI-CNN	85.4	88.0	65.1	79.5	77.5	81.8	50.8	70.0	66.5	76.5	61.6	68.2	58.9	72.1	60.7	63.9
MV-TC	77.3	<u>88.9</u>	54.2	73.5	63.5	84.0	36.6	61.4	65.7	79.2	65.9	70.3	59.5	77.3	51.8	62.9
PI-TC	81.2	<u>88.9</u>	<i>74.1</i>	<i>81.4</i>	71.5	<i>84.2</i>	41.4	65.7	<i>69.3</i>	<i>77.5</i>	<u>91.1</u>	79.3	63.8	76.7	<i>61.8</i>	<i>67.4</i>
MV-Proxy	79.7	89.6	37.1	68.8	66.1	<u>85.1</u>	35.0	62.1	63.2	78.3	<u>53.6</u>	65.0	57.9	74.7	49.3	60.6
PI-Proxy	<u>85.1</u>	88.7	66.1	80.0	79.9	<u>85.1</u>	40.6	68.5	68.7	<u>80.0</u>	70.8	73.2	62.6	<u>78.2</u>	49.4	63.4
PiRO-SE (Ours)	<u>85.1</u>	88.1	82.9	85.4	78.9	82.9	61.9	74.6	69.6	80.3	88.4	79.4	65.8	75.6	68.5	70.0
PiRO-DE (Ours)	<u>85.0</u>	88.3	94.1	89.1	<u>79.3</u>	85.3	84.5	83.0	70.2	82.5	93.1	81.9	<u>65.2</u>	82.8	80.6	76.2

Table 2. Comparison of performance on pose-invariant classification and retrieval tasks on the ObjectPI and ModelNet-40 datasets with the state-of-the-art approaches. The best, second-best, and third-best performance is highlighted in bold, underline, and italics respectively. The methods starting with MV indicate multi-view methods and those starting with PI indicate methods that learn pose invariant embeddings. For our method PiRO, SE and DE stands for single and dual embedding spaces. The average classification and retrieval performance indicate that we learn better representations for recognition and retrieval tasks on both datasets. The improvements in single-view object recognition and retrieval performance are the most significant.

Method	Classification (Accuracy %)				Retrieval (mAP %)			
	SV Cat	MV Cat	SV Obj	Avg	SV Cat	MV Cat	SV Obj	Avg
PI-CNN	79.7	83.3	23.6	62.2	70.2	76.8	10.5	52.5
PI-Proxy	80.0	83.2	23.4	62.2	70.6	77.0	10.7	52.8
PI-TC	76.1	82.5	36.5	65.0	61.5	74.7	15.9	50.7
Ours	78.9	81.8	83.0	81.2	68.0	74.2	72.8	71.7

Table 3. Comparison of performance on the FG3D dataset with state-of-the-art pose-invariant methods.

ing category-specific embeddings and do not effectively separate the embeddings for objects within each category. In contrast, our proposed pose-invariant object loss separates confusing instances of objects from the same category which helps learn more discriminative fine-grained features to distinguish between visually similar objects resulting in significant improvement on single-view object recognition accuracy of 46.5% and object retrieval mAP of 56.9%. Overall, we outperform the pose-invariant methods on the classification tasks by 16.2% and retrieval tasks by 18.9%.

(C) Ablation Studies:

Visualization of pose-invariant embeddings: From Fig. 5, we observe that for the pose-invariant methods (PI-CNN,

PI-Proxy, and PI-TC), the embeddings for objects from the same category are not well-separated leading to poor performance on object-based tasks. In contrast, the object embeddings generated using our method are much better separated as our pose-invariant object loss separates confusing instances of objects from the same category. A more detailed comparison is shown in Supplemental Sec. 6.

Single and dual embedding spaces: From Tables 1 and 4, we observe that learning dual embeddings leads to better overall performance, especially for object-based tasks. This is because, for category-based tasks, we aim to embed objects from the same category close to each other while for object-based tasks, we aim to separate objects apart from each other to be able to discriminate between them. This leads to contradicting goals for object and category-based tasks in the single embedding space. Learning dual embeddings more effectively captures category and object-specific attributes in separate representation spaces leading to overall performance improvements.

Pose-invariant losses: We employ three losses in PiRO: \mathcal{L}_{cat} to distinguish between different categories, \mathcal{L}_{picat} for clustering objects from the same category, and \mathcal{L}_{piobj} for clustering different views of the same object and separating

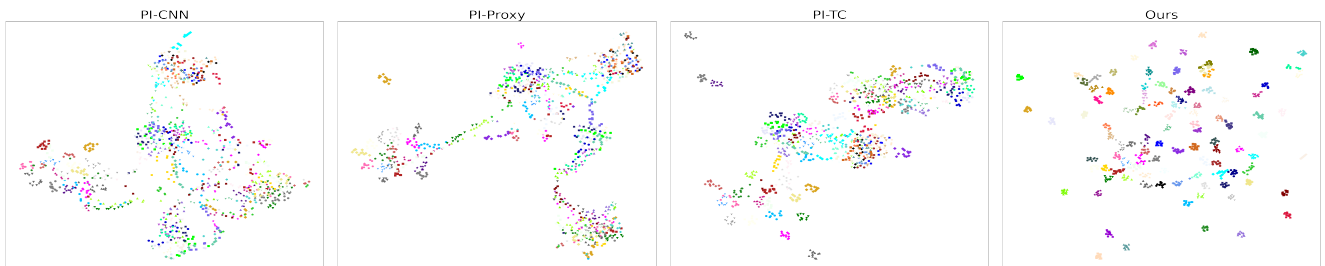


Figure 5. We show UMAP [13] visualizations for a qualitative comparison of the object embedding space learned for the ModelNet40 test dataset (from 5 categories such as table, desk, chair, stool, and sofa with 100 objects) by prior pose-invariant methods [7] and our method. Each instance is an object view and a unique color and shape is used to denote each object-identity class in the visualizations.

Dataset	Embed. Space	Losses	Classification (Accuracy %)					Retrieval (mAP %)				
			Category		Object		Avg.	Category		Object		Avg.
			SV	MV	SV	MV	Avg.	SV	MV	SV	MV	Avg.
ObjectPI	Single	\mathcal{L}_{cat}	70.7	81.6	78.7	87.8	79.7	65.3	82.9	54.8	92.9	73.9
		$\mathcal{L}_{cat} + \mathcal{L}_{piobj}$	69.4	81.6	88.5	98.0	84.4	66.0	75.6	68.5	98.9	77.2
	Dual	$\mathcal{L}_{cat} + \mathcal{L}_{piobj} + \mathcal{L}_{picat}$	71.2	82.7	83.3	95.9	83.3	65.6	82.8	62.3	98.0	77.2
		$\mathcal{L}_{cat} + \mathcal{L}_{piobj}$	71.2	82.7	94.5	99.0	86.8	65.7	82.9	80.5	99.5	82.2
ModelNet40	Single	\mathcal{L}_{cat}	84.7	88.4	71.3	75.9	80.1	79.0	84.8	45.3	82.0	72.8
		$\mathcal{L}_{cat} + \mathcal{L}_{piobj}$	85.4	88.8	81.2	85.6	85.2	79.1	83.1	59.2	90.4	78.0
	Dual	$\mathcal{L}_{cat} + \mathcal{L}_{piobj} + \mathcal{L}_{picat}$	84.7	88.4	71.8	79.3	81.0	78.7	84.9	49.1	85.2	74.5
		$\mathcal{L}_{cat} + \mathcal{L}_{piobj}$	84.5	88.6	94.6	96.6	91.1	78.9	85.0	85.2	98.1	86.8
FG3D	Single	\mathcal{L}_{cat}	79.3	81.8	18.2	19.0	49.5	66.6	73.1	9.7	28.4	44.5
		$\mathcal{L}_{cat} + \mathcal{L}_{piobj}$	78.3	80.2	26.2	31.0	53.9	64.9	69.0	15.7	42.9	48.1
	Dual	$\mathcal{L}_{cat} + \mathcal{L}_{piobj} + \mathcal{L}_{picat}$	78.4	81.1	29.3	41.8	57.6	65.1	70.8	17.9	55.0	52.2
		$\mathcal{L}_{cat} + \mathcal{L}_{piobj}$	78.7	82.2	83.2	91.4	83.9	67.6	73.1	72.8	95.3	77.2
Dual	$\mathcal{L}_{cat} + \mathcal{L}_{piobj} + \mathcal{L}_{picat}$	79.0	81.9	83.1	91.6	83.9	68.1	74.4	73.0	95.5	77.8	

Table 4. Ablations of the proposed losses in the single and dual embedding spaces.

confusing instances from different objects of the same category for object-based tasks. Table 4 shows that in the single embedding space, \mathcal{L}_{cat} is effective for category-based tasks, but not for object-based tasks. Adding \mathcal{L}_{piobj} improves performance in object-based tasks, but at the cost of category-based tasks (especially MV category retrieval). This can be mitigated by adding \mathcal{L}_{picat} that enhances performance on category-based tasks. However, \mathcal{L}_{picat} and \mathcal{L}_{piobj} have conflicting objectives in the same space and only marginally improve overall performance over \mathcal{L}_{cat} in the single embedding space. In the dual embedding space, these losses are optimized in separate embedding spaces. In the dual space, we observe that $\mathcal{L}_{cat} + \mathcal{L}_{piobj}$ improves overall performance, particularly for object-based tasks, and adding \mathcal{L}_{picat} boosts performance on category-based tasks and yields the best overall performance for all the datasets. \mathcal{L}_{piobj} enhances the separability of object-identity classes facilitating learning more discriminative object embeddings that significantly improves performance on object-based tasks (see detailed ablation study of \mathcal{L}_{piobj} in Sup. Sec 7).

Optimizing intra-class and inter-class distances: In the top of Fig. 6, we show the maximum intra-class distance (d_{intra}^{max}) and minimum inter-class distance (d_{inter}^{min}) between object-identity classes from the same category during training on the ModelNet40 dataset. These distances are computed using the object-identity embeddings and averaged

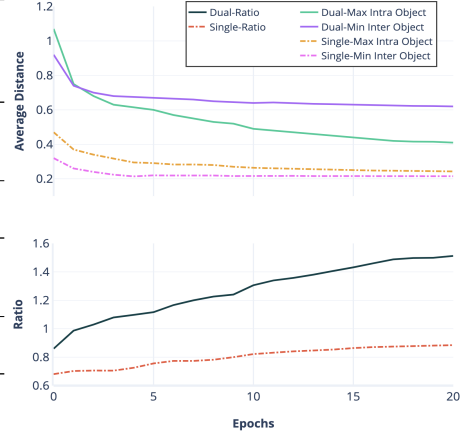


Figure 6. Optimization of the inter-class and intra-class distances for object-identity classes during training while learning single and dual embedding spaces for the ModelNet40 dataset.

over all objects. We also plot the ratio $\rho = \frac{d_{inter}^{min}}{d_{intra}^{max}}$ in the bottom of Fig. 6. A higher ρ value indicates embeddings of the same object-identity class are well clustered and separated from embeddings of other object-identity classes from the same category. Comparing the plots for the single and dual embedding spaces, we observe that ρ and d_{inter}^{min} are much higher for the dual space indicating better separability of object-identity classes when learning a dual space. We observe the same effect for all datasets (see Sup. Sec 8).

Embedding dimensionality: In Fig. 7, we observe that for ModelNet-40, a dimension of 64 for category and 128 for object-level tasks is sufficient for good performance. For ObjectPI, higher dimensions of 256 and 512 are required for category and object-level tasks respectively to capture color and texture information in addition to shape, unlike ModelNet-40. A higher embedding dimensionality is required for object-level tasks compared to category-level tasks possibly because object embeddings need to capture finer details to effectively distinguish between objects. We provide more details in the Supplemental Sec. 9.

Qualitative results: In the Supplemental, we illustrate how self-attention captures correlations between different views of an object using multi-view attention maps in Sec. 10, and present qualitative object retrieval results in Sec. 11.

5. Conclusion

We propose a multi-view dual-encoder architecture and pose-invariant ranking losses that facilitate learning discriminative pose-invariant representations for joint category and object recognition and retrieval. Our method outperforms state-of-the-art methods on several pose-invariant classification and retrieval tasks on three publicly available multi-view object datasets. We further provide ablation studies to demonstrate the effectiveness of our approach.

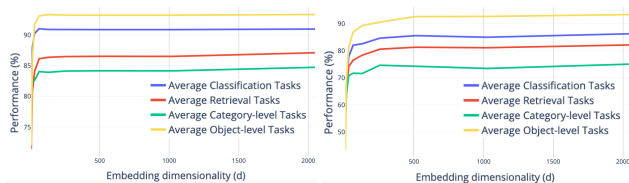


Figure 7. Effect of embedding dimensionality on performance.

References

- [1] W. Chen, X. Chen, J. Zhang, and K. Huang. Beyond triplet loss: A deep quadruplet network for person re-identification. In *Computer Vision and Pattern Recognition (CVPR)*, pages 1320–1329, 2017. 2
- [2] S. Chopra, R. Hadsell, and Y. LeCun. Learning a similarity metric discriminatively, with application to face verification. In *Computer Vision and Pattern Recognition (CVPR)*, pages 539–546 vol. 1, 2005. 2
- [3] Alexey Dosovitskiy, Lucas Beyer, Alexander Kolesnikov, Dirk Weissenborn, Xiaohua Zhai, Thomas Unterthiner, Mostafa Dehghani, Matthias Minderer, Georg Heigold, Sylvain Gelly, Jakob Uszkoreit, and Neil Houlsby. An image is worth 16x16 words: Transformers for image recognition at scale. In *International Conference on Learning Representations (ICLR)*, 2021. 3
- [4] Weifeng Ge, Weilin Huang, Dengke Dong, and Matthew R. Scott. Deep metric learning with hierarchical triplet loss. In *European Conference on Computer Vision (ECCV)*, pages 272–288. Springer International Publishing, 2018. 2
- [5] B. Harwood, V. Kumar B.G., G. Carneiro, I. Reid, and T. Drummond. Smart mining for deep metric learning. In *International Conference on Computer Vision (ICCV)*, pages 2840–2848, Los Alamitos, CA, USA, 2017. IEEE Computer Society. 2
- [6] Xinwei He, Yang Zhou, Zhichao Zhou, Song Bai, and Xiang Bai. Triplet-center loss for multi-view 3d object retrieval. *Computer Vision and Pattern Recognition (CVPR)*, 2018. 2, 6
- [7] Chih-Hui Ho, Pedro Morgado, Amir Persekian, and Nuno Vasconcelos. Pies: Pose invariant embeddings. In *Computer Vision and Pattern Recognition (CVPR)*, 2019. 1, 2, 3, 6, 7, 10, 11, 12
- [8] Elad Hoffer and Nir Ailon. Deep metric learning using triplet network. *Lecture Notes in Computer Science*, page 84–92, 2015. 2
- [9] Chen Huang, Chen Change Loy, and Xiaoou Tang. Local similarity-aware deep feature embedding. In *Neural Information Processing Systems (NeurIPS)*, page 1270–1278, Red Hook, NY, USA, 2016. Curran Associates Inc. 2
- [10] Asako Kanezaki, Yasuyuki Matsushita, and Yoshifumi Nishida. Rotationnet: Joint object categorization and pose estimation using multiviews from unsupervised viewpoints. *Computer Vision and Pattern Recognition (CVPR)*, pages 5010–5019, 2018. 2
- [11] Weiyang Liu, Yandong Wen, Zhiding Yu, and Meng Yang. Large-margin softmax loss for convolutional neural networks. In *International Conference on Machine Learning (ICML)*, page 507–516. JMLR.org, 2016. 5
- [12] Xinhai Liu, Zhizhong Han, Yu-Shen Liu, and Matthias Zwicker. Fine-grained 3d shape classification with hierarchical part-view attentions. *IEEE Transactions on Image Processing*, 2021. 6
- [13] Leland McInnes, John Healy, Nathaniel Saul, and Lukas Großberger. Umap: Uniform manifold approximation and projection. *Journal of Open Source Software*, 3(29):861, 2018. 7
- [14] Yair Movshovitz-Attias, Alexander Toshev, Thomas K Leung, Sergey Ioffe, and Saurabh Singh. No fuss distance metric learning using proxies. In *International Conference on Computer Vision (ICCV)*, pages 360–368, 2017. 2
- [15] Weizhi Nie, Yue Zhao, Dan Song, and Yue Gao. Dan: Deep-attention network for 3d shape recognition. *IEEE Trans. on Image Processing*, 30:4371–4383, 2021. 3
- [16] Omkar M. Parkhi, Andrea Vedaldi, and Andrew Zisserman. Deep face recognition. In *British Machine Vision Conference (BMVC)*, pages 41.1–41.12. BMVA Press, 2015. 2
- [17] Rohan Sarkar, Navaneeth Bodla, Mariya Vasileva, Yen-Liang Lin, Anurag Beniwal, Alan Lu, and Gerard Medioni. Outfittransformer: Outfit representations for fashion recommendation. In *Computer Vision and Pattern Recognition Workshops (CVPRW)*, pages 2263–2267, 2022. 3
- [18] Rohan Sarkar, Navaneeth Bodla, Mariya I. Vasileva, Yen-Liang Lin, Anurag Beniwal, Alan Lu, and Gerard Medioni. Outfittransformer: Learning outfit representations for fashion recommendation. In *Winter Conference on Applications of Computer Vision (WACV)*, pages 3601–3609, 2023. 3
- [19] Florian Schroff, Dmitry Kalenichenko, and James Philbin. Facenet: A unified embedding for face recognition and clustering. *Computer Vision and Pattern Recognition (CVPR)*, 2015. 2
- [20] Karen Simonyan and Andrew Zisserman. Very deep convolutional networks for large-scale image recognition. In *International Conference on Learning Representations (ICLR)*, 2015. 6
- [21] Hyun Oh Song, Yu Xiang, Stefanie Jegelka, and Silvio Savarese. Deep metric learning via lifted structured feature embedding. In *Computer Vision and Pattern Recognition (CVPR)*, pages 4004–4012, 2016. 2
- [22] Hang Su, Subhransu Maji, Evangelos Kalogerakis, and Erik G. Learned-Miller. Multi-view convolutional neural networks for 3d shape recognition. In *International Conference on Computer Vision (ICCV)*, 2015. 2, 6
- [23] Yumin Suh, Bohyung Han, Wonsik Kim, and Kyoung Mu Lee. Stochastic class-based hard example mining for deep metric learning. In *Computer Vision and Pattern Recognition (CVPR)*, pages 7244–7252, 2019. 2
- [24] Xun Wang, Haozhi Zhang, Weilin Huang, and Matthew R Scott. Cross-batch memory for embedding learning. In *Computer Vision and Pattern Recognition (CVPR)*, pages 6388–6397, 2020. 2
- [25] X. Wei, Y. Gong, F. Wang, X. Sun, and J. Sun. Learning canonical view representation for 3d shape recognition with arbitrary views. In *2021 IEEE/CVF International Conference on Computer Vision (ICCV)*, pages 397–406, Los Alamitos, CA, USA, 2021. IEEE Computer Society. 3
- [26] Zhirong Wu, S. Song, A. Khosla, Fisher Yu, Linguang Zhang, Xiaoou Tang, and J. Xiao. 3d shapenets: A deep representation for volumetric shapes. In *Computer Vision and Pattern Recognition (CVPR)*, pages 1912–1920, Los Alamitos, CA, USA, 2015. IEEE Computer Society. 2, 5
- [27] Hong Xuan, Abby Stylianou, Xiaotong Liu, and Robert Pless. Hard negative examples are hard, but useful. In *European Conference on Computer Vision (ECCV)*, pages 126–142. Springer International Publishing, 2020. 2

Dual Pose-invariant Embeddings: Learning Category and Object-specific Discriminative Representations for Recognition and Retrieval

Supplementary Material

In the supplementary material, we present additional results that could not be reported in detail in the main paper due to space constraints. Our supplemental is organized as follows. In Sec. 6, we present UMAP visualizations of the learned pose-invariant embeddings for the ObjectPI, ModelNet40, and FG3D datasets. In Sec. 7, we present a detailed ablation study of the different components of the proposed pose-invariant object loss. We investigate how the inter-class and intra-class distances for the object-identity classes are optimized in the object embedding space, and further explain how the separation of object-identity classes leads to significant performance improvement on object-level tasks. Furthermore, we investigate how the object-identity classes are better separated when learning dual embedding spaces as compared to a single embedding space in Sec. 8. Subsequently in Sec. 9, we study the effect of embedding dimensionality on category and object-based classification and retrieval tasks. Next, we illustrate how self-attention captures correlations between different views of an object using multi-view attention maps in Sec. 10,

and finally present qualitative single-view object retrieval results in Sec. 11.

6. UMAP visualization of pose-invariant embeddings

For a qualitative understanding of the effectiveness of our approach, we compare the embeddings generated by the prior pose-invariant methods (specifically, PI-CNN, PI-Proxy, and PI-TC) in [7] with our method. For this, we use UMAP to project the embeddings into the 2-dimensional space for visualization. In Fig. 8, we compare the UMAP plots for a subset of the test dataset of ModelNet-40. Since ModelNet-40 has a large number of objects in the test dataset, we choose 100 objects for visualization from five mutually confusing categories such as tables and desks, chairs, stools, and sofas. In the category plots, we use five distinct colors to indicate instances from each of the five categories. In the object plots, instances of each object-identity class are indicated by a unique color and shape.

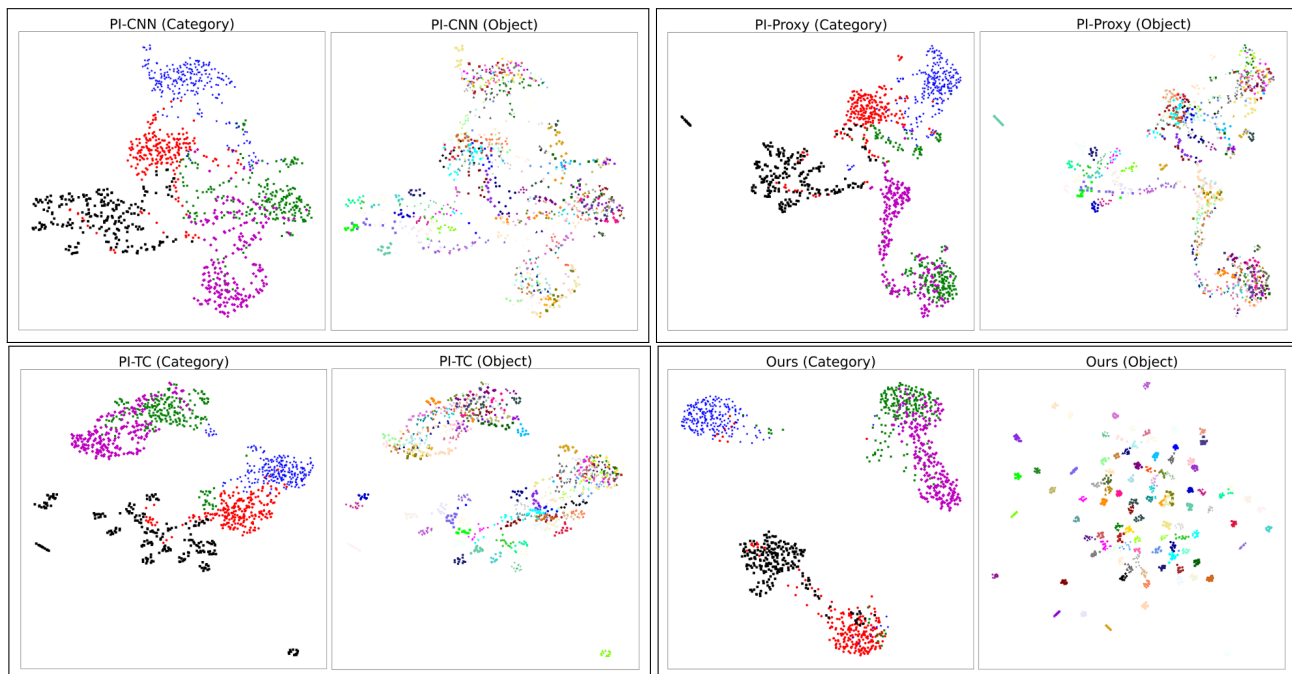


Figure 8. Qualitative comparison of the embedding space learned for a subset of the ModelNet40 test dataset (from 5 categories such as table, desk, chair, stool, sofa with 100 objects) by prior pose-invariant methods [7] and our method (bottom-right). In the category plots (to the left of each subfigure), we use five distinct colors to indicate instances from each of the five categories. In the object plots (to the right of each subfigure), instances of the same object-identity class are indicated by a unique color and shape.

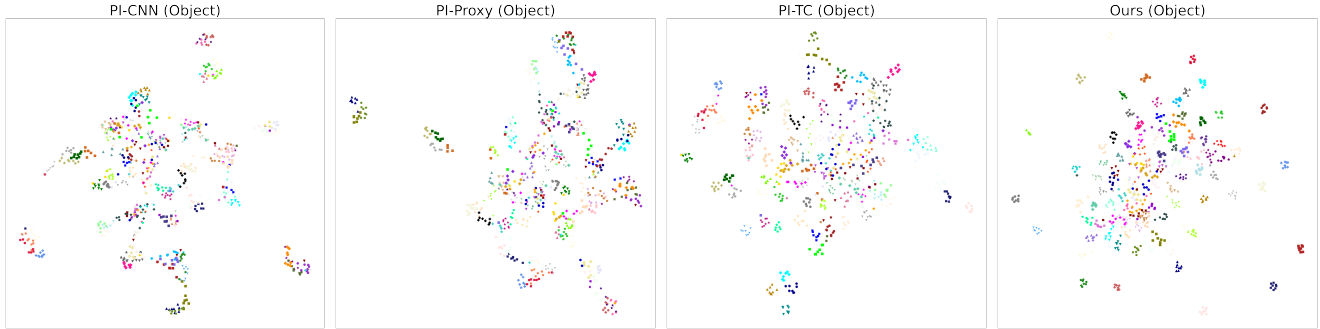
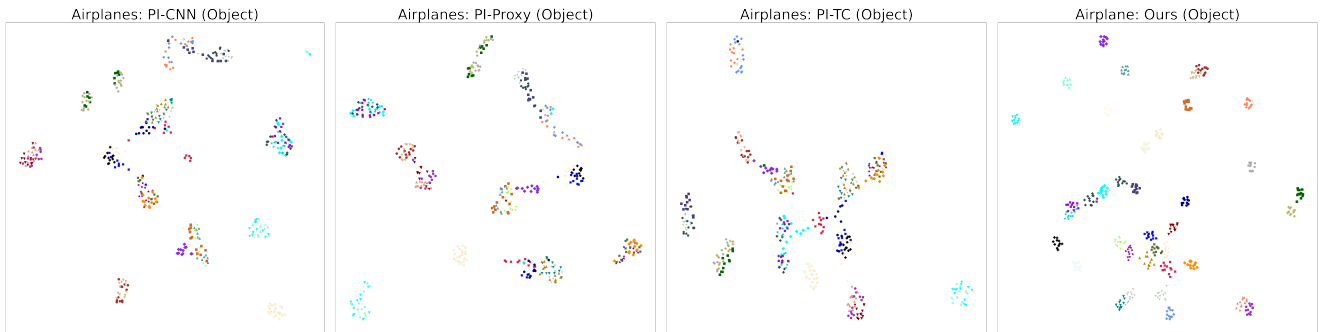
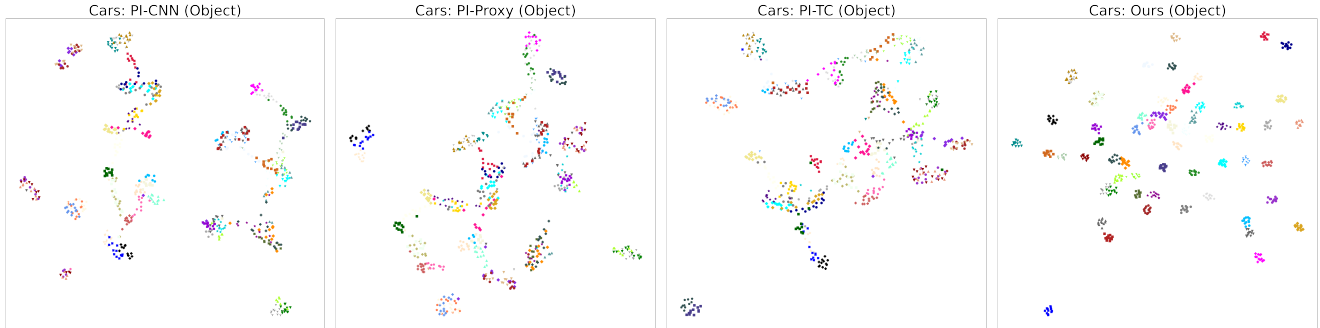


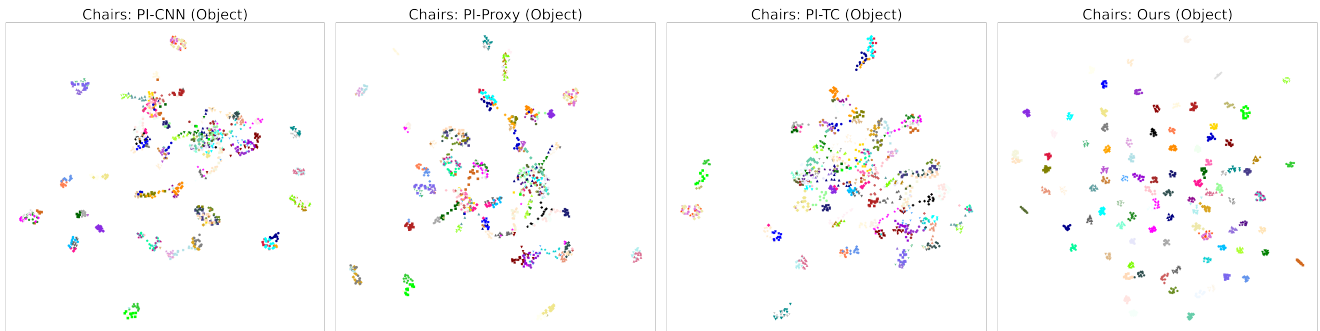
Figure 9. Comparison of the object embedding space learned for the ObjectPI test dataset (with 98 objects) by prior pose-invariant methods [7] and our method (right). Each instance is an object view and each object-identity class is denoted by a unique color and shape.



(a) Object-identity embeddings for 39 airplane objects (3 objects each from 13 airplane categories)



(b) Object-identity embeddings for 60 car objects (3 objects each from 20 car categories)



(c) Object-identity embeddings for 99 chair objects (3 objects each from 33 chair categories)

Figure 10. Comparison of the object embedding space learned for the FG3D test dataset (comprising objects with fine-grained differences from 13 airplane categories in (a), 20 car categories in (b), and 33 chair categories in (c)) by prior pose-invariant methods [7] and our method (right). Each instance is an object view and each object-identity class is denoted by a unique color and shape. It can be observed that our object-identity embeddings are better clustered and separated from other objects as compared to prior methods.

Prior pose-invariant methods (PI-CNN, PI-Proxy, and PI-TC) in [7] learn a single embedding space. For each of these methods, we show the UMAP visualizations of the same embedding space with the category and object-identity labels in the two subfigures (titled category and object). As mentioned in the paper, prior work focused primarily on learning category-specific embeddings, with the object-to-object variations within each category represented by the variations in the embedding vectors within the same embedding space. Specifically, we observe that for PI-CNN and PI-Proxy (in the top row of Fig. 8), the pose-invariant embeddings for object-identity classes belonging to the same category are not well-separated leading to poor performance on object-based tasks reported in the main paper in Tables 2, 3. PI-TC (bottom-left of Fig. 8) separates embeddings of the nearest neighbor object-identity classes in the embedding space leading to comparatively better performance.

In contrast, our method decouples the category and object representations in separate embedding spaces leading to a better separation of both the category and object-identity embeddings, as can be seen in the bottom-right of Fig. 8. The most notable difference with prior state-of-the-art is in regards to the learnt object-identity embeddings. Hence, for the other datasets we compare the object-identity embeddings generated by our method and prior pose-invariant methods. In Fig. 9, we visualize the embeddings for the ObjectPI test dataset comprising 98 objects from 25 categories. The FG3D dataset has 66 fine-grained categories that comprise 13 types of airplanes, 20 types of cars, and 33 types of chairs. We sample 3 objects per category and show the object-identity embeddings for the airplane, car, and chair objects separately in Fig. 10 (a), (b), and (c) respectively. For all the datasets, we observe that the object-identity classes are better clustered and separated for our method as compared to prior methods.

We conjecture that our method better separates the object-identity classes for two reasons. First, our method separates confusing instances of objects from the same category that would otherwise be much too close together in the embedding space, as we will explain in detail in Section 7. Second, our method captures category and object-specific discriminative features in separate embedding spaces. Intuitively, this allows us to simultaneously capture common attributes between objects from the same category in the category embedding space and discriminative features to distinguish between them in the object embedding space, as opposed to learning representations to satisfy these conflicting objectives in the same embedding space. This strategy leads to better separability of the object-identity embeddings when learning a dual space as compared to learning a single space, as we will explain in detail in Section 8.

7. Ablation of Pose-invariant object loss

As explained in Sec. 2(B) of the main paper, prior approaches primarily focus on clustering the single-view embeddings of each object-identity class close to their multi-view embeddings but do not effectively separate embeddings from different object-identity classes. To ameliorate this, our proposed pose-invariant object loss is designed to separate different object-identity classes, and in this section, we investigate its importance for good performance on object-based tasks.

Our pose-invariant object loss in Eqn. 8 has two components – clustering loss (\mathcal{L}_{intra}) that reduces the intra-object distances by clustering different views of the same object-identity class, similar to prior approaches. Additionally, we add a separation loss (\mathcal{L}_{inter}) that increases the inter-object distances by separating confusing instances of different object-identity classes from the same category. To understand the effectiveness of each component, we train

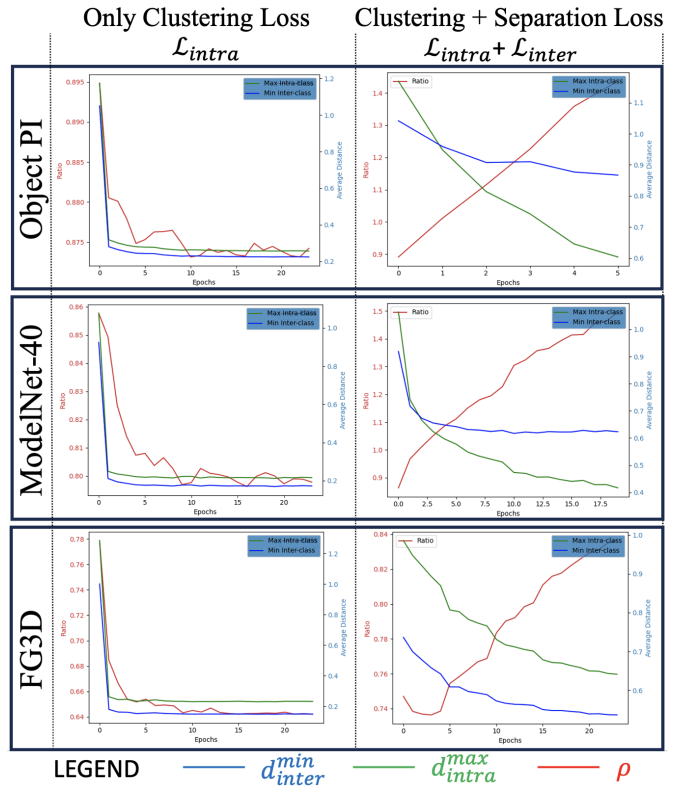


Figure 11. This figure illustrates how the minimum inter-class distances between object-identity classes (d_{inter}^{min} in blue), maximum intra-class distances (d_{intra}^{max} in green), and the ratio of the two distances (ρ in red) change as the different components of our pose-invariant object loss are optimized for all three datasets. When training using the clustering loss only, ρ decreases. Whereas, when training using both the losses together, ρ increases indicating better compactness and separability of object-identity classes.

Datasets	Losses	Optimized distances during training			Test Performance on Object-level tasks			
		$d_{intra}^{max} (\downarrow)$	$d_{inter}^{min} (\uparrow)$	$\rho (\uparrow)$	Classification (Acc. %)		Retrieval (mAP %)	
					Single-view	Multi-view	Single-view	Multi-view
ObjectPI	\mathcal{L}_{intra}	0.26	0.23	0.87	84.9	87.8	59.8	93.2
	$\mathcal{L}_{intra} + \mathcal{L}_{inter}$	0.60	0.90	1.50	92.7	98.0	81.0	99.0
ModelNet-40	\mathcal{L}_{intra}	0.22	0.18	0.80	68.5	68.6	43.0	76.2
	$\mathcal{L}_{intra} + \mathcal{L}_{inter}$	0.41	0.62	1.51	93.7	96.9	84.0	98.2
FG3D	\mathcal{L}_{intra}	0.23	0.15	0.65	20.2	24.4	10.4	34.7
	$\mathcal{L}_{intra} + \mathcal{L}_{inter}$	0.63	0.53	0.84	83.1	91.6	73.0	95.5

Table 5. This table shows the maximum intra-class and minimum inter-class distances between object-identity classes after training, and also the test performance on single-view and multi-view object recognition and retrieval tasks for the three datasets, when training with and without the separation loss.

the PAN encoder with and without the separation loss. We track how the intra-class and inter-class distances are optimized during training in Fig. 11, and also the performance on object recognition and retrieval tasks in Table 5.

In Fig. 11, we plot the maximum intra-class distance (d_{intra}^{max} in green), and the minimum inter-class distance between object-identity classes from the same category (d_{inter}^{min} in blue) during training to monitor the compactness and separability of object-identity classes respectively. These distances are computed using the object-identity embeddings and averaged over all objects. We also plot the ratio $\rho = \frac{d_{inter}^{min}}{d_{intra}^{max}}$ in red. A lower d_{intra}^{max} , and higher d_{inter}^{min} and ρ values would indicate embeddings of the same object-identity class are well clustered and separated from embeddings of other object-identity classes from the same cate-

gory.

We observe that training using the clustering loss (\mathcal{L}_{intra}) reduces the d_{intra}^{max} as it encourages clustering different views of the same object-identity together encouraging the network to learn pose-invariant features. However, only using the clustering loss also reduces d_{inter}^{min} , thereby reducing ρ as can be observed in the left of Fig. 11. Therefore, the object-identity classes are not well separated as can be seen in the left of Fig. 12, and this results in poor performance on object-level tasks.

Whereas, when training using the clustering and separation loss jointly ($\mathcal{L}_{intra} + \mathcal{L}_{inter}$), we observe in the right of Fig. 11 that ρ increases as the d_{inter}^{min} decreases at a much slower rate than d_{intra}^{max} , and d_{inter}^{min} eventually converges to a value beyond which it does not decrease substantially, indicating that our loss enforces separability between objects from the same category. For all the datasets, adding the separation loss yields significant performance improvement on object-level tasks, as can be seen in Table 5. This is because it enhances the inter-object separability that allows the encoder to learn more discriminative features to distinguish between visually similar objects. This can be observed in the right of Fig. 12, where each distinct object-identity class (indicated by a unique color and shape) can be more easily distinguished from other object-identity classes.

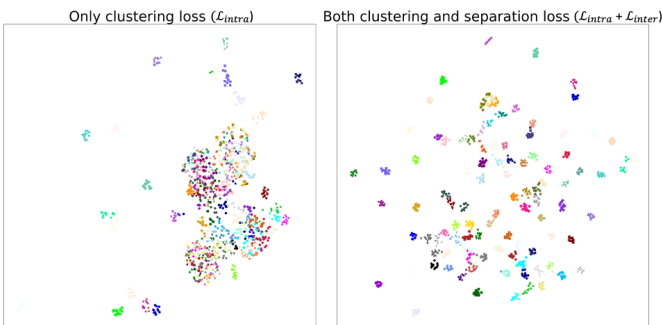


Figure 12. We show the object-identity embeddings for a total of 100 objects from 5 categories of ModelNet-40 (20 objects from each category, such as tables, desks, chairs, stools, and sofas). The instances of each object-identity class is indicated by a unique color and shape. This figure illustrates that only clustering embeddings of the same object-identity classes is not sufficient to be able to distinguish between different object-identities, especially when there are many visually similar objects (left). Clustering the different views of the same object-identity classes, and simultaneously separating the different object-identity classes encourages learning more discriminative embeddings (right).

8. Optimizing intra-class and inter-class distances in single and dual spaces

As mentioned in the previous section, the pose-invariant object loss is designed to simultaneously enhance the inter-class separability and intra-class compactness of object-identity classes. In this section, we study how the distances between the samples in the object embedding space are optimized during training when learning single and dual embedding spaces.

For comparison, we show how these distances are optimized when learning representations in a single and dual embedding spaces, at the top and bottom of Fig. 13(A), (B),

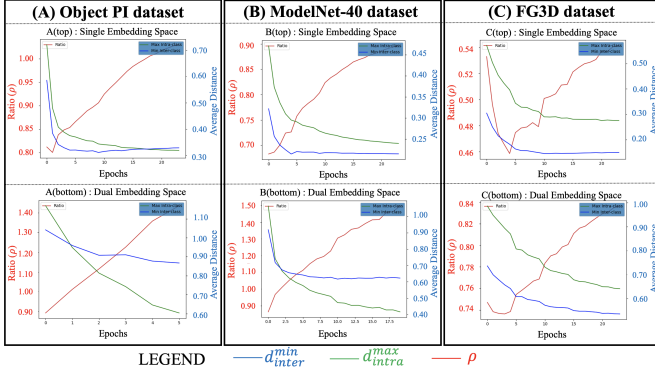


Figure 13. For all three datasets, this figure illustrates that our pose-invariant object loss increases the ratio ρ that indicates better separability and compactness of object-identity classes. We observe that the values of the ratio ρ (in red) and the minimum inter-class distance d_{inter}^{min} (in blue) are higher when learning a dual space as compared to a single space. This indicates better separation between object-identity classes when learning in the dual space.

and (C) for the ObjectPI, ModelNet-40, and FG3D datasets respectively. We observe that the values of ρ and the minimum inter-object distances (d_{inter}^{min}) are much higher in the dual space, which indicates that the object embeddings in the dual embedding space are better separated than those in the single embedding space, leading to better performance on object-based tasks, as shown in Table 6.

Fig. 14 illustrates this effect using UMAP visualizations of the embeddings in single and dual spaces. As mentioned in the paper, we jointly train our encoder using pose-invariant category and object-based losses. In the single embedding space, category-based losses aim to cluster embeddings of object-identity classes from the same category together, and in the same embedding space, the object-based loss aims to separate different object-identity classes from the same category. Due to these conflicting objectives in

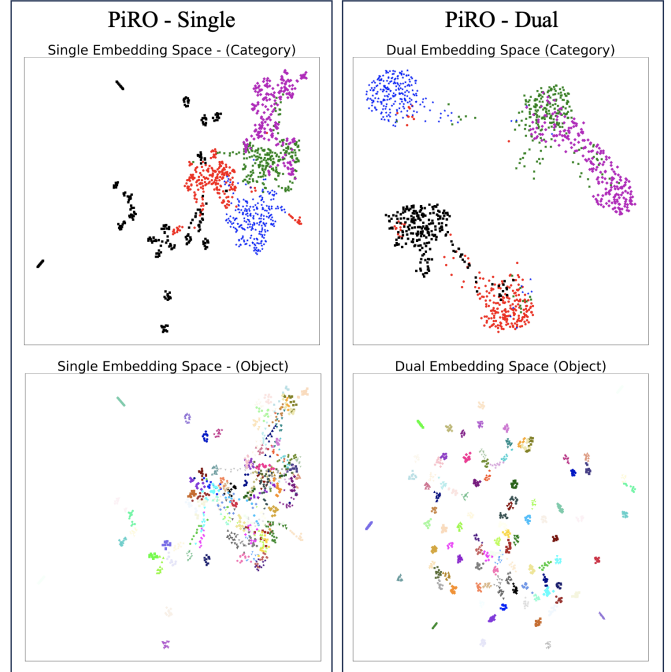
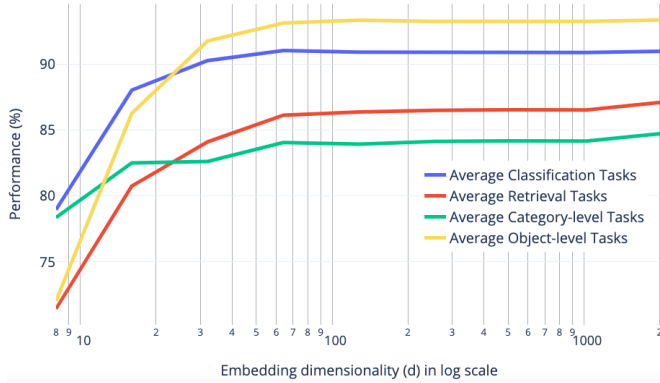


Figure 14. UMAP visualization of the 100 objects from 5 different categories of ModelNet-40 for the single embedding space (left) and dual embedding space (right). The figure illustrates that decoupling the category and object-identity representations in separate spaces leads to better separability between categories in the category embedding space and object-identity classes in the object embedding space (right) as compared to learning representations in the same embedding space (left).

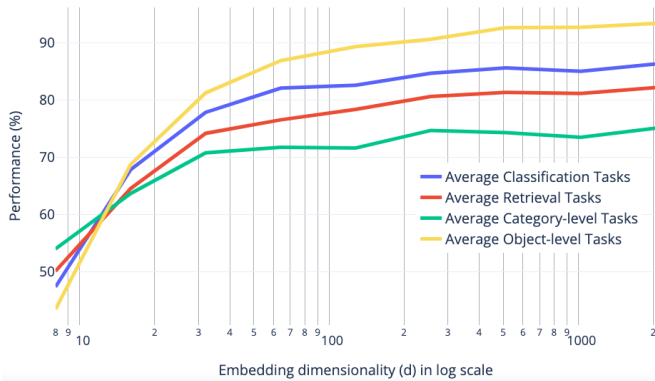
the same embedding space, object-identity classes are not separated well, as can be seen in Fig. 14 (left). In the dual space, the category and object representations are decoupled, and the category and object losses optimize the distances in the separate embedding spaces. As can be seen in Fig. 14 (right), the object and category embeddings are

Datasets	Embedding Space	Optimized distances during training			Test Performance on Object-level tasks			
		$d_{intra}^{max} (\downarrow)$	$d_{inter}^{min} (\uparrow)$	$\rho (\uparrow)$	Classification (Acc. %)		Retrieval (mAP %)	
					Single-view	Multi-view	Single-view	Multi-view
ObjectPI	Single	0.32	0.33	1.03	88.5	98.0	68.5	98.9
	Dual	0.60	0.90	1.50	92.7	98.0	81.0	99.0
ModelNet-40	Single	0.24	0.22	0.92	81.2	85.6	59.2	90.4
	Dual	0.41	0.62	1.51	93.7	96.9	84.0	98.2
FG3D	Single	0.29	0.16	0.55	26.2	31.0	15.7	42.9
	Dual	0.63	0.53	0.84	83.1	91.6	73.0	95.5

Table 6. This table shows the maximum intra-class and minimum inter-class distances between object-identity classes after training when learning a single and dual embedding space. We observe that the d_{inter}^{min} and ρ values are higher in the dual embedding space indicating better separability of object-identity classes in the object embedding space. This yields better performance on object-level tasks for all the three datasets.



(a) ModelNet-40 dataset



(b) ObjectPI dataset

Figure 15. This graph illustrates the effect of embedding dimensionality on Average Classification and Retrieval performance for category and object-based tasks for ModelNet-40 (top) and ObjectPI (bottom) datasets.

much better separated and we learn more discriminative embeddings overall in the dual space. This leads to significant performance improvements on object-based tasks, as can be seen in Table 6.

9. Embedding dimensionality

For this experiment, we varied the embedding dimensionality from $d = 8, 16, \dots, 2048$ for the category and object embedding space. We measured the performance of our method in terms of the average classification and retrieval performance as well as average performance on category-based and object-based tasks.

From Fig. 15, we observe that the performance on all four metrics improves with an increase in embedding dimensionality but beyond a certain embedding dimension, the performance only improves marginally. For the ModelNet-40 dataset, we observe that $d = 64$ for category-based tasks and $d = 128$ for object-based tasks is sufficient. For the ObjectPI dataset, we observe that $d = 256$

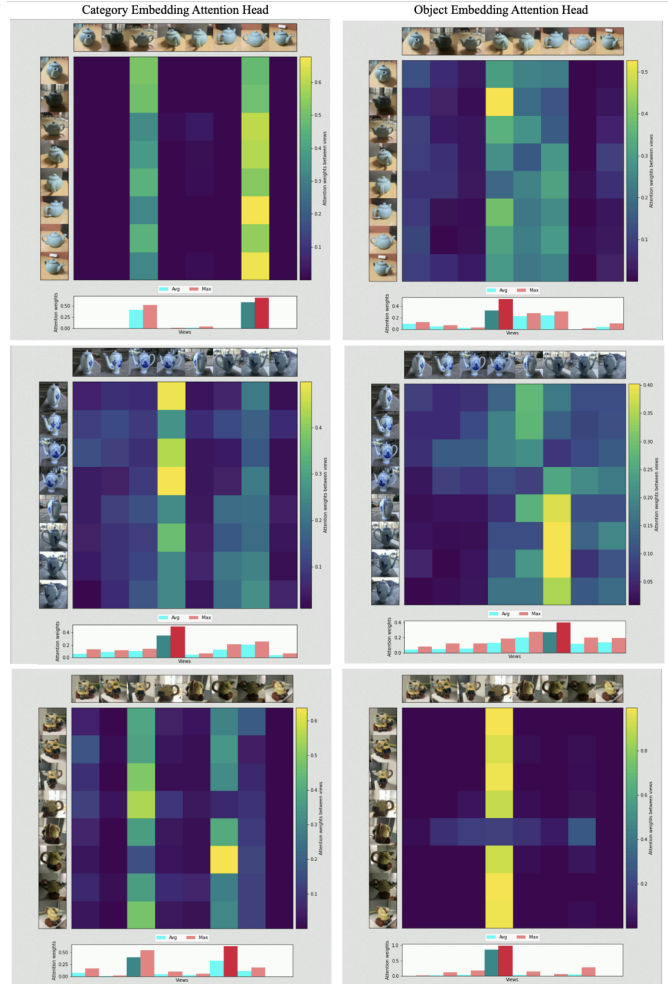


Figure 16. Visualization of multi-view attention maps for the category and object self-attention layers.

and $d = 512$ are sufficient for category-based and object-based tasks. We conjecture that higher embedding dimensionality is required for ObjectPI than ModelNet-40 as the embeddings for ObjectPI need to additionally capture color and texture information instead of just shape information for ModelNet-40. In general, the embedding dimensionality required for good performance on object-based tasks is higher than on category-based tasks as object embeddings need to capture more fine-grained details to differentiate between objects.

10. Multi-view attention maps

We plot the attention weights for the self-attention layers for the object and category embeddings in Figure 16. We observe that for category embeddings, the attention weights are higher for representative views that capture the overall shape of the kettle. All views of the object are correlated

to these representative views. For object embeddings, we observe that the attention weights are higher for the views that capture attributes related to the handle. This is possibly because the different kettles in the dataset have variations in the location (from the top or side) and shape of the handle.

11. Qualitative Retrieval Results

We show some qualitative object retrieval results on ObjectPI and ModelNet40 datasets in Figs. 17 and 18 respectively. The single-view object retrieval results show that given an arbitrary view of the object, our method can retrieve the other views of the same object correctly in Figs. 17 and 18. Despite variability in object appearance from different viewpoints, the presence of similar objects in the database as well as deformable objects (such as books, clothing, and so on), our method can retrieve objects with high precision.

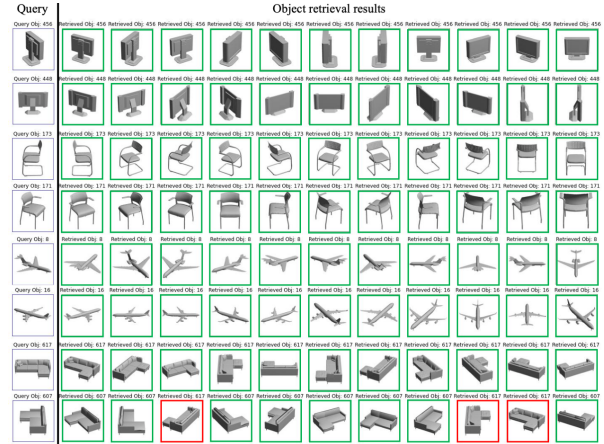


Figure 18. For a single-view query in each row, the retrieved images of other views of the same object are shown on the right for the ModelNet40 dataset. The green and red bounding boxes indicate correct and wrong results respectively.



Figure 17. This figure shows our object retrieval results for the Object PI dataset. Given a single view query from an arbitrary pose on the left, the top-7 retrieved results are shown on the right in each row. Green bounding boxes indicate correct retrieval results and red boxes indicate incorrect results. In (a), we demonstrate that our framework can identify retrieve other views of the same object despite having similar objects in the test dataset. In (b), we demonstrate, despite significant appearance changes under various pose transformations for different everyday objects, our framework can retrieve objects accurately.